SCIENTIFIC REPORTS

OPEN

SUBJECT AREAS:
SEISMOLOGY
GEOPHYSICS

Received
25 June 2014

Accepted
22 July 2014

Published
26 August 2014

Correspondence and requests for materials should be addressed to F.M. (francesco.mulargia@unibo.it.)

Anthropogenic Triggering of Large Earthquakes

Francesco Mulargia[1] & Andrea Bizzarri[2]

[1]Università degli Studi di Bologna, Dipartimento di Fisica e Astronomia, Viale Carlo Berti Pichat, 6/2– 40127 Bologna – Italy, [2]Istituto Nazionale di Geofisica e Vulcanologia, Sezione di Bologna, Via Donato Creti, 12 – 40128 Bologna – Italy.

The physical mechanism of the anthropogenic triggering of large earthquakes on active faults is studied on the basis of experimental phenomenology, i.e., that earthquakes occur on active tectonic faults, that crustal stress values are those measured in situ and, on active faults, comply to the values of the stress drop measured for real earthquakes, that the static friction coefficients are those inferred on faults, and that the effective triggering stresses are those inferred for real earthquakes. Deriving the conditions for earthquake nucleation as a time-dependent solution of the Tresca-Von Mises criterion applied in the framework of poroelasticity yields that active faults can be triggered by fluid overpressures < 0.1 MPa. Comparing this with the deviatoric stresses at the depth of crustal hypocenters, which are of the order of 1–10 MPa, we find that injecting in the subsoil fluids at the pressures typical of oil and gas production and storage may trigger destructive earthquakes on active faults at a few tens of kilometers. Fluid pressure propagates as slow stress waves along geometric paths operating in a drained condition and can advance the natural occurrence of earthquakes by a substantial amount of time. Furthermore, it is illusory to control earthquake triggering by close monitoring of minor "foreshocks", since the induction may occur with a delay up to several years.

The central role of fluids in seismic faulting is known in all stages of the earthquake cycle, i.e., in the nucleation processes, in the dynamic propagation and in the post-seismic evolution. Namely, pore fluid pressure affects the whole earthquake process starting from fault nucleation[1,2], continues through thermally-activated pressurization[3–7] and mechanical lubrication[8,9], and finally plays a role in triggering aftershocks[10–14]. Interest on the first step of the process (fault reactivation and rupture nucleation) has been recently revived by several cases of human activities, which are indicted for having induced destructive earthquakes. Davies et al.[15] compiled a list of 190 possible examples of induced earthquakes, with magnitude spanning between 1.0 and 7.9, connected with mining, artificial reservoir impoundment, geothermal operations[16,17], oil and gas field production and hydraulic fracturing (i.e., fracking).

Most earthquakes induced by anthropogenic activities concern small magnitude events ($M < 3.0$) located in the vicinity of the activities themselves[18,19]. Here we are not interested in such earthquakes, which generally constitute more a nuisance than a real danger. Indeed, we are interested in the other type of induced seismicity, which regards *large events* ($M > 5.5$) on nearby active tectonic faults, at a distance up to a few tens of kilometers[20,21]. This type of induction is appropriately termed *triggered* (or *activated*) *seismicity*[22], since human activities provide the tiny — but fundamental — input to a system which is independently close to instability. A small action produces a large reaction, just as the modest pressure of a finger on a gun trigger releases the large explosive energy stored in the propellant. Such a type of induced seismicity has been so far mostly associated with the impoundment of artificial water reservoirs, but occasionally also with gas and oil production.

Triggered seismicity is the most important and dangerous type of induced seismicity, and should not be confused with its stablemate, simply called *induced seismicity*; the latter is commonly associated with drilling or hydrofracture and generally implies large local stresses, but small earthquakes. In fact, to induce fresh fracture in the bulk rock the applied stresses must be, by definition, equal to those determined by hydrofracture techniques. However, event size is small because these large stresses are spatially concentrated and can only induce fracture on small volumes of rock. On the contrary, triggered seismicity involves large tectonic structures, where the stress has been independently accumulating to a near failure conditions by the internal Earth's dynamics[23,24], with the human activity providing only the "last straw".

Although the unequivocal discrimination between naturally occurring and man-triggered earthquakes is difficult[25,26], there exist some hardly questionable cases. The first documented case of reservoir-triggered seismicity occurred in 1932 in Algeria's Oued Fodda Dam. Another prominent example is provided by the realization of the Koyna Dam, India, which was followed in 1967 by the M6.5 Koynanagar earthquake, where 180 people died

and 1,500 were injured[27]. Other relevant cases are the M6.1 Oroville, California, earthquake, also attributed to a reservoir, and the M5.4 Aswan, Egypt, earthquake in 1981[21], which occurred 15 years after the filling of the Nasser artificial lake. The largest and most recent case of reservoir triggered earthquakes is possibly that of the Zipingpu Dam in China, which is indicted for triggering the May 12 2008 M7.9 Wenchuan earthquake, killing some 80,000 people[28–30].

Dams are most often at the root of man-triggered seismicity, but there are some notable additions. Caused by the injection of pressurized fluids into a 367-m-deep borehole at the Rocky Mountain Arsenal, Colorado was the Denver earthquake sequence in the '60s, which culminated in a M5.3 event[31]. The injection of pressurized fluids to stimulate the production of an oil field, induced a M5.4 earthquake in Caviaga, Italy, in 1951[32], and may have also triggered the earthquake sequence of May 20-29 2012 in Emilia, Italy, with two events of M6.0 and another five above M5.3, which resulted in the death of 27 people as well as a major wound to the gasping Italian economy[33,34].

The physical problem of quantifying the man-triggering mechanism is a problem still lacking a comprehensive approach, even if the basic constitutive equations have been known since quite long ago. We work out a solution on the basis of the following phenomenological ingredients:

1) *Time invariance*; since the time scale of earthquake recurrence on the same fault segment is 100-1000 years and the evolution of the driving mechanism is a geological process 3–4 order of magnitudes slower, earthquakes can be taken as repetitions on existing weakness zones — the *faults*.
2) *Stress on faults are close to failure by an unknown extent*; the stress history on faults depends on the interaction with neighboring faults and on a variety of factors practically impossible to quantify.
3) *Low static friction coefficients*; static friction on fault zones is much lower than in bulk (undamaged) rocks and in the laboratory (cf.[35]), and has values $\mu < 0.3$[36–41].
4) *Very low stress thresholds for triggering*; additional fluid pressures of 0.05 MPa due to artificial water reservoirs have activated destructive earthquakes[17]; similar low values occur in the dynamic triggering by nearby earthquakes[42,43].
5) *Earthquakes triggered with considerable time delay*; earthquakes have been triggered with time delays > 10 years[17,21].
6) *Earthquakes triggered at considerable distance in space*; earthquakes have been triggered at up to 30 kilometers[17,21].

According to such phenomenological constraints, earthquake triggering is likely to occur only on the most favorably oriented pre-existent faults, which are at an angle θ to the largest (in norm) principal stress. This angle is given by $\theta = \frac{1}{2}\mathrm{arctg}\left(\frac{1}{\mu}\right)$, i.e., according to the above-mentioned values of μ, it is comprised in the 37°–45° range. Given that the exact μ values are impossible to know beforehand, we consider the asymptotic limit $\mu \to 0$, which corresponds to the maximum shear stress orientation of 45° to the largest principal stress. In addition, among the optimally oriented faults, only those in close proximity to failure will be triggered. In this framework, we can write the failure criterion as[1,44,45]:

$$\sigma^{eff} = \frac{\sigma^{\mathrm{I}} - \sigma^{\mathrm{III}}}{2} - \mu\left(\frac{\sigma^{\mathrm{I}} + \sigma^{\mathrm{III}}}{2} - p_{fluid}\right) \quad (1)$$

$$\sigma^{eff} > \sigma_R \quad (2)$$

where μ formally is the static friction coefficient (often written as μ_u or μ_s in the literature), σ^{I} and σ^{III} are the first and third principal stresses, respectively. p_{fluid} is pore fluid pressure, which we will consider in the range 100–150% of the hydrostatic load (see Numerical results and discussion of the failure threshold section). In other words, we assume that under normal conditions the fluid is in the hydrostatic pressure thanks to a drained percolation-driven circulation[46], and we consider the perturbation due to an externally induced pore fluid pressure increase. The failure stress σ_R is a material property, which we assume to be fixed. By keeping μ constant, we implicitly assume that it represents an average value over the whole fault surface (i.e. we neglect any possible effect of spatial heterogeneities). Moreover, equation (1) also disregards any possible coupling with temperature variations and second-order effects[47–49].

When fluids are injected into the system, p_{fluid} is increased, thus increasing σ^{eff} (equation (1)), which may then reach the failure condition (equation (2))[50–52] on a nearby fault which is independently close to failure. We study the problem by first considering a time independent model to establish the failure threshold and then we consider the time evolution of the process.

A time independent model

In reservoirs, water is stored in artificial lakes inducing in the ground a fluid pressure equal to the hydrostatic column. Typically, the depth h of these artificial basins is some tens of meters and therefore the additional overpressure they induce in the subsoil, $\rho_{fluid}\, g\, h$ is of the order of 0.1 MPa. In a similar manner, pressurized fluids — basically water — are injected into ageing gas and oil fields to increase the percentage of the extracted oil or gas — the so-called *recovery factor* – or to maintain the productivity over longer periods. In other cases, gas (either methane for storage or CO_2 for sequestration and disposal) is injected in the fluids, resulting in overpressures up to a fraction of the ambient fluid pressure.

While the exact values of p_{fluid} and its evolution depend on each specific case, we consider overpressures up to 50% of the hydrostatic pressure:

$$p_{fluid} = (1+\alpha)\, p_{hydro} = (1+\alpha)\, \rho_{fluid}\, g\, z \quad (3)$$

z being the depth with respect to the ground surface. Such a wide range of values of α ($\alpha = 0$–0.5) can be considered exhaustive of most operational configurations.

Fluid pressures as low as 0.01 MPa have been suggested capable to trigger earthquakes[37,53], while fluid pressures of 0.05 MPa have been experimentally found to trigger[17]. We consider a "conservative" threshold of 0.1 MPa, a value that can be safely stated as capable of earthquake triggering. Comparing this value with the ambient stress of ~ 300 MPa at a depth of ~ 10 km, typical of M5.5 crustal earthquake hypocenters, we find that the earthquake triggering stresses are comparatively very small (roughly 0.03%), a conclusion consistent with the values independently inferred for static and dynamic aftershock induction[42,43].

We take as crustal stress values those determined by in situ measurements (e.g.[54,55]; for a comprehensive source see also[56]), which yield that the stresses in the crust are well approximated by a nearly lithostatic condition, i.e., by stresses $\sigma_{ij} = \delta_{ij}\, \sigma_V \sim 27$ MPa km^{-1}, and deviatoric stresses are of the order of 10 MPa km^{-1}, or 100 MPa at 10 km depth. However, the in situ stresses were measured on bulk rock and *not* on faults, even if in some cases not far from them. The deviatoric stress values on faults can be directly inferred from the stress drop as follows. While the experimental in situ static friction coefficients are very low, the dynamic friction coefficients will be[57] equally low — or lower — implying that earthquakes release virtually all deviatoric stresses. Hence, on faults, the latter must be equal to the stress drop, which is of the order of 1–10 MPa[58,59]. Using such values, the principal stresses on faults remains essentially lithostatic with a minor perturbation (cf. equation (4)), i.e. fluid pressure makes faults reside always in a state close to failure, in agreement with the *criticality* paradigm (for a comprehensive treatment see e.g.[45]). In other words, during an earthquake "cycle" the deviatoric stresses vary only within 0.3–3% of the ambient stress, so that any reliable estimate of

time-dependent risk of failure would require to know the state of stress on the fault with a practically unrealizable accuracy. Hence, we must prudentially assume that all faults neighboring the anthropogenic activity are so close to instability that they will fail when σ^{eff} increases by 0.1 MPa due to an increment in fluid pressure. This condition namely replaces the rupture condition expressed by equation (2).

Numerical results and discussion of the failure threshold

Since our primary goal is to provide a quantitative inference on the possible rupture initiation, we merely evaluate if the rupture condition is met, i.e., if the Tresca-Von Mises criterion is satisfied. We use typical *in situ* stress values[54–56]:

$$\begin{aligned} \sigma^{\mathrm{I}} - \sigma^{\mathrm{III}} &= 1 \text{ MP km}^{-1} \\ \sigma^{\mathrm{I}} + \sigma^{\mathrm{III}} &= 53 \text{ MPa km}^{-1} \end{aligned} \text{, normal faulting}$$

$$\begin{aligned} \sigma^{\mathrm{I}} - \sigma^{\mathrm{III}} &= 1 \text{ MPa km}^{-1} \\ \sigma^{\mathrm{I}} + \sigma^{\mathrm{III}} &= 54 \text{ MPa km}^{-1} \end{aligned} \text{, thrust faulting.} \qquad (4)$$

The results are shown in figure 1, where we report the effective stress σ^{eff} as a function of the depth z for a 25% overpressure with respect to the hydrostatic pressure. The picture shows[3] that for both compressive (red curves) and normal faults (blue) earthquake induction is possible with static friction coefficients lower than 0.2, with marginally lower thresholds for the latter. It is also important to note that effective stress, and therefore the induction capability, increases linearly with depth, in agreement with the experimental evidence that triggered earthquakes tend not to have a superficial source[20,21,34].

Figure 2 shows the effective stress as a function of overpressure, i.e., of p_{fluid} normalized to the hydrostatic pressure, at a depth of 5 kilometers. Earthquake induction appears to be crucially affected by both the static friction coefficient and overpressure. The balance is subtle, with activation not occurring for faults with a μ larger than 0.25 at whatever overpressure and occurring only at overpressures above 30% for $\mu = 0.2$. For lower friction coefficients activation is possible for all values of overpressure, and failure occurs already at 0%, i.e., when pore fluid is at the mere hydrostatic pressure, emphasizing the role of precipitation in triggering earthquakes[60]. The activation of strike-slip faults is bound to be an intermediate case between the normal and compressive cases, and depends on the detail of the local conditions. Note that the increase in effective stress reaches easily values which are a large fraction of the stress drop — approximately 2 MPa in effective stress per 10% increase in fluid pressure (see Fig. 2) — implying a possible triggering of *all* faults, and not only of the mature ones, with a substantial advance of the occurrence time.

Summing up, the time-independent solution candidates fluid pressurization as the basic ingredient for earthquake triggering. We now proceed to study how the process evolves with time.

A time-dependent solution

So far, we have considered a time-independent increase in pore fluid pressure, controlled by the overpressure parameter α. The complementary time-dependent problem concerns how a time-varying p_{fluid} at a given spatial source perturbs the fluid pressure field as a function of time in the surrounding region. We must solve a coupled elastic-hydraulic problem in which fluid migration plays a fundamental role. This problem, which can be tackled in the domain of poroleasticity[61,62], has been already studied by several authors[17,46,63–65] in connection with the seismicity induced by the pore pressure increase due to a change in the level of a reservoir lake behind a dam. In a 2-D model, the total pore pressure at a depth z, distance x and time t, $p(r,t)$, can be expressed as the superposition of the coupled response of diffused pore pressure and undrained pore pressure as (ibid.):

$$p(r,t) = \gamma\, p_0 \,\mathrm{erf}\left(\frac{r}{2\sqrt{\omega t}}\right) + p_0 \,\mathrm{erfc}\left(\frac{r}{2\sqrt{\omega t}}\right) \qquad (5)$$

where p_0 is the input pressure at the time $t = 0$, ω the hydraulic diffusivity and $r = (x^2 + z^2)^{1/2}$ the pressure-source to fault distance, and γ the relative weight of the drained and undrained contributions, which in a porous solid under laboratory conditions can be expressed as a function of the Skempton coefficient B and of the undrained Poisson modulus v_u: $\gamma = B\,\frac{1+v_u}{3\,(1-v_u)}$.

However, under real crustal Earth's conditions the effective value of γ depends on the pattern of faults that rule the draining, which occurs essentially through the "easy paths" rather than the bulk pores. While knowing beforehand the existence — and the geometry — of such a connected pattern is impossible, most authors have found that only assuming its existence, i.e. $\gamma \sim 0$, allows a satisfactory fit to the data[10,17,46,63–65]. In a similar fashion, while hydraulic diffusivity of crustal rocks varies experimentally in the laboratory and the field over 16 decades[64], its effective value in the cases of triggered seismicity ranges only over 2 decades, from 0.1 to 10 $m^2\ s^{-1}$ [46].

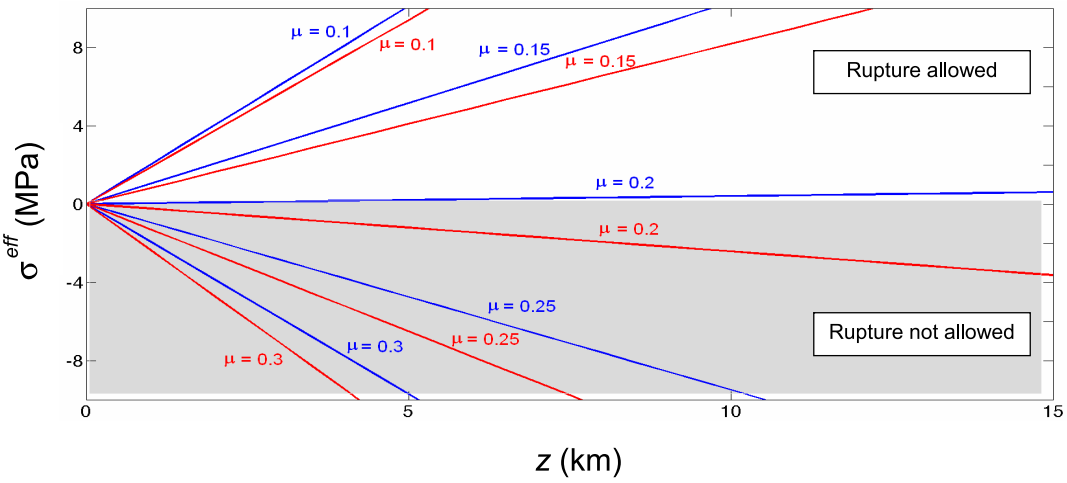

Figure 1 | The effective stress σ^{eff} as a function of depth z for a 25% overpressure with respect to the hydrostatic (i.e., $\alpha = 0.25$) for different values of the static friction coefficient μ. Values of σ^{eff} are computed through equations (1), (3) and (4). Blue curves stand for normal faults and red curves for compressive faults. The grey shaded area stands for the region where rupture is not possible.

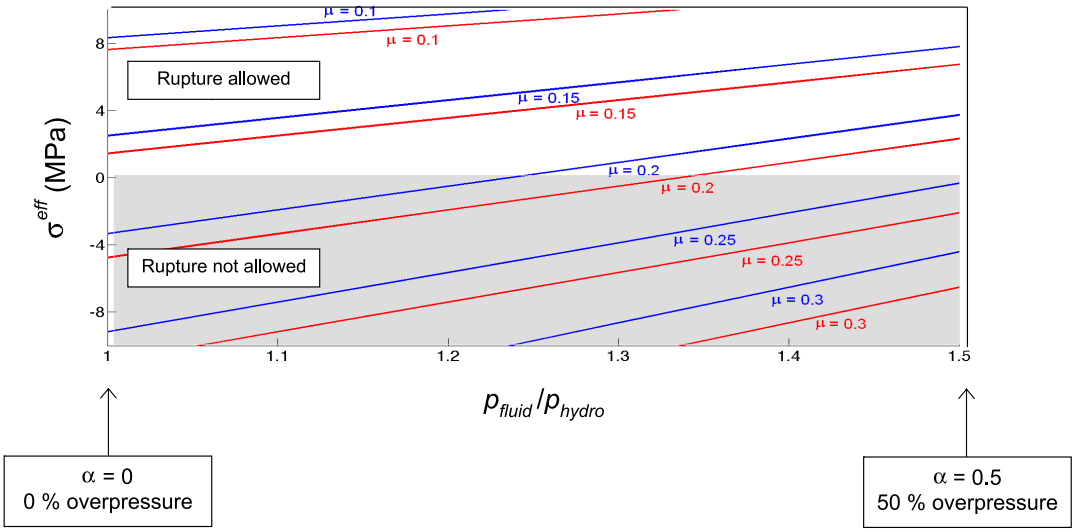

Figure 2 | The effective stress as a function of overpressure for different values of the static friction coefficient μ at a depth of 5 kilometers. As in the previous figure, blue curves stand for normal faults and red curves for compressive faults. The grey shaded area still denotes the region where rupture is not possible.

We consider here the application to two practical cases, both involving an input fluid pressure varying with time, one relative to a "short" time scale and another to a "long" time scale. In these cases, when the input pore pressure p_0 is time-dependent, the solution can be obtained from equation (5) by the principle of superposition at different initial times. Figure 3 shows the short time scale case, with the input (blue curve) and pore pressures at 1, 2, 4 and 6 km from the injection point (red curves), normalized to the input pressure. Its main feature — well known in all the cases of triggered earthquakes — is the delay with which the pore pressure "wave" propagates. In fact, we find that fluid pressure in the crust propagates as a wave: the pressure will increase and then die away. Note the difference with a simple (and intuitive) steady state solution: in that case pressure will increase and then stay at a high value. The peak pressure (marked with arrows in Fig. 3) occurs always well after the input pressure decrease has begun (in other words, when the pressurization has been already terminated); at 1 km it occurs right after the end of the full load interval, at 2 km 60 days later, while at 4 km and 6 km it occurs nearly 100 and almost 150 days later, when the input pressure is below 50% of its maximum. This is important, since it shows how early warning procedures to promptly halt the pressurization can hardly be effective. Concerning the pore pressures, these reach values

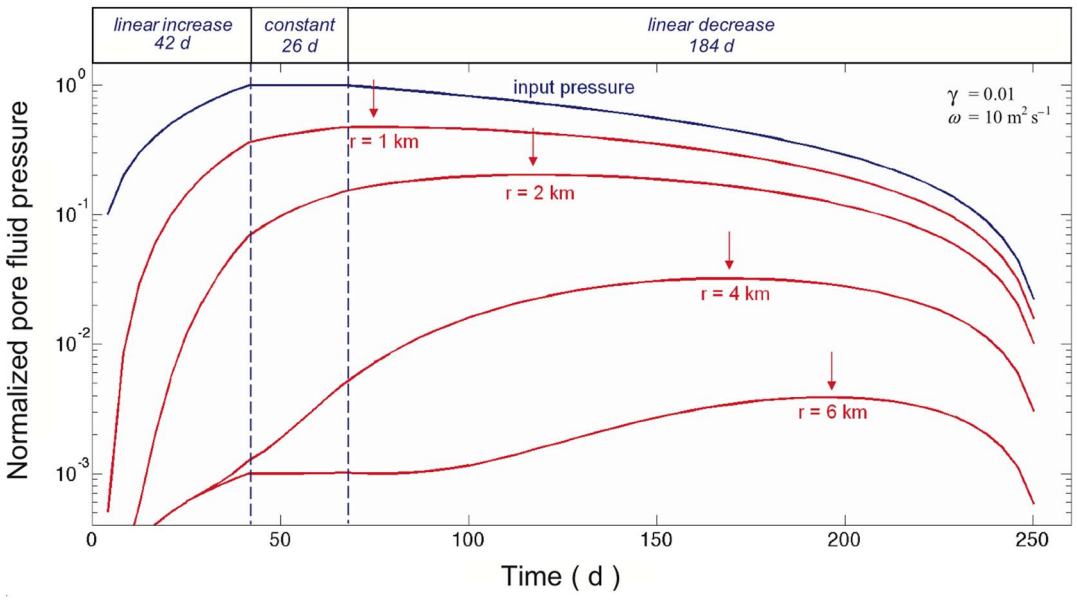

Figure 3 | Results pertaining to the fluid diffusion. The input and the resulting pore pressures (blue and red curves, respectively), normalized to the former as a function of time at different times and distances $r = (x^2 + z^2)^{1/2}$ from the injection point relative to a "short" time scale. Arrows indicate the peaks in the resulting pore pressure, which is given by equation (5). The input pressure increases from 0 to its maximum according to a linear ramp 42 days long, it stays constant for 26 days and goes back to 0 according to a linear ramp lasting 184 days. The horizontal portion of this input signal (i.e., where it reaches its maximum value) is associated with the values given by equation (3), and thus it is ultimately related to a specific value of the overpressure parameter α. More complicated input time functions can be handled, but the present choice, which describes realistic operational conditions, makes it possible to capture the most important features of the problem. A value of $\gamma = 0.01$ was assumed together with a hydraulic diffusivity $\omega = 10$ m^2 s^{-1}.

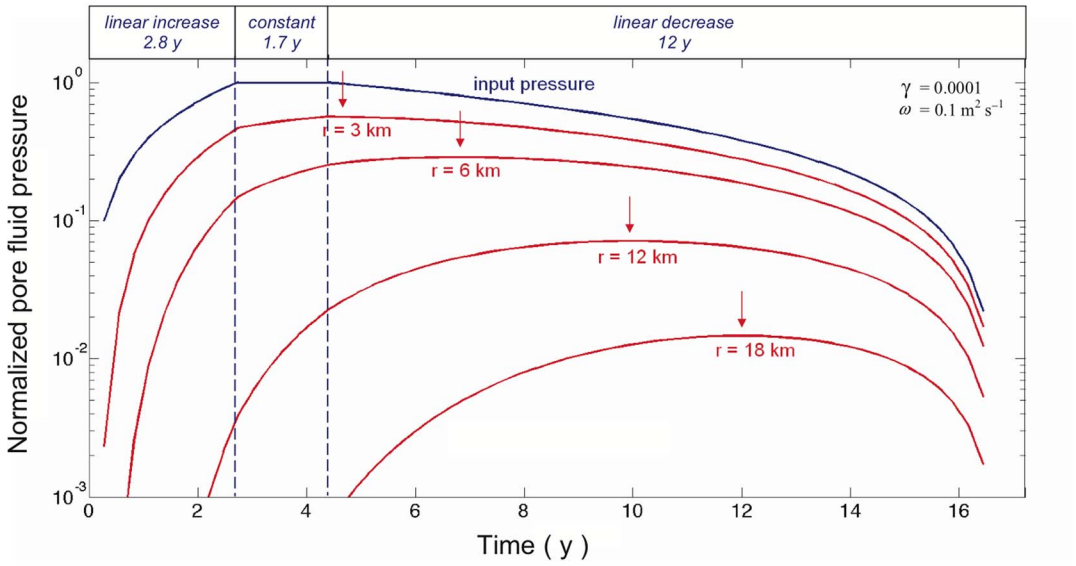

Figure 4 | The same as Fig. 3, but relative to a "long" time scale. It concerns an input pressure increasing from 0 to its maximum according to a linear ramp 2.8 years long, followed by a constant load for 1.7 years and going back to 0 according to a linear ramp lasting 12 years. A value of $\gamma = 0.0001$ was assumed together with a hydraulic diffusivity $\omega = 0.1$ m^2 s^{-1}.

larger than 20% of the maximum input pressure at distances less than 2 km, but are respectively one and two orders of magnitude smaller at 4 and 6 km. The pore pressure curve at 6 km from the injection point shows initially the predominance of the undrained elastic term, with an increase almost simultaneous with the load, and then, after more than 100 days, the delayed arrival and predominance of the hydraulic pressure wave.

Figure 4 shows the "long" time scale case, with the input and pore pressures computed at 3, 6, 12 and 18 km from the injection point, still normalized by the input pressure. Again, the picture is dominated by the delayed propagation of the pore pressure wave, which reaches its peak value 8 and 10 years after the input at 12 km and 18 km, respectively, attaining pressure values which are within some percent of the input. Remarkably, the latter values are only apparently small, if one recalls that hydrostatic pore fluid pressure at hypocentral depths is 3 orders of magnitude larger than the stresses found to trigger earthquakes near reservoirs (see A time independent model section).

Discussion and conclusions

Considering the case of induced seismicity relative to large destructive earthquakes, we found that they are due to small fluid overpressures which trigger nearby tectonic faults. Pulling the trigger of loaded gun is an action minute *per se*, but decisive for shooting. The same earthquakes would occur naturally, but at a (possibly much) later time, due to an increase in the shear stress induced by tectonic loading, to stress perturbations from slip on neighboring faults, to the fluid overpressure of a nearby earthquake, or the dynamic load imposed by the waves of the same. The time required to naturally achieve the failure depends on a variety of factors, starting from the load rate and the residual stress left over by previous earthquakes. Since the "recurrence" time of earthquakes on the same fault segment is of the order of 10^3 years[66–68] and since the stress drop is of the order of 1–10 MPa[58,59,69,70], the threshold we used places the lower limit of anthropogenic advance in the time of occurrence at some decades, but the calculated values of the effective stresses yield that the *clock advance* (see, e.g., Fig. 2 of[24] and references cited therein) can be very substantial.

The effect of this anthropogenic perturbation is like anticipating the death of a living organism to a sooner date than that which would naturally occur; as such, it carries some potential societal responsibilities. Another important issue emerging from the above results is that there is little hope to control triggered seismicity through an early warning based on intensive monitoring: the pore pressure wave propagates with such a delay that no matter how fast one reacts to the onset of minor precursory seismicity, he will be too late (see A time-dependent solution section). In fact, the fluid pressure pulse propagates independently of what is done at the source. Actually, it may still be propagating even after the whole apparatus that produced it has been not only shut off, but also dismantled.

To recap, as pointed out by[71] and reiterated by[31,72–75] and many others, the fact that fluid injection into the ground may trigger tectonic earthquakes has been known for quite long[76,77], although the combined lack of a thorough comprehension of the basic mechanisms has possibly prevented considering them always with the due caution. Indeed, a general policy which maximizes the oil and gas recovery and storage and concurrently minimizes the risks of fluid injection has still to be defined. Any project should primarily include a detailed mapping of nearby active faults, carefully evaluating the seismic risk and — if the case — proceeding to secure the region prior to any operation.

1. Sibson, R. H. Frictional constraints on thrust, wrench and normal faults. *Nature* **249**, 542–544 (1974).
2. Sibson, R. H. Brecciation processes in fault zones: Inferences from earthquake rupturing. *Pure Appl. Geophys.* **124**, 169–175 (1986).
3. Sibson, R. H. Interaction between temperature and pore-fluid pressure during earthquake faulting —A mechanism for partial or total stress relief. *Nature* **243**, 66–68 (1973).
4. Lachenbruch, A. H. Frictional heating, fluid pressure, and the resistance to fault motion. *J. Geophys. Res.* **85**, 6097–6122 (1980).
5. Andrews, D. J. A fault constitutive relation accounting for thermal pressurization of pore fluid. *J. Geophys. Res.* **107**, No. B12, 2363, doi:10.1029/2002JB001942 (2002).
6. Mulargia, F., Castellaro, S. & Ciccotti, M. Earthquakes as three stages processes. *Geophys. J. Int.* **158**, 98–108, doi:10.1111/j.1365-246X.2004.02262.x (2004).
7. Bizzarri, A. & Cocco, M. A thermal pressurization model for the spontaneous dynamic rupture propagation on a three-dimensional fault: 1. Methodological approach. *J. Geophys. Res.* **111**, B05303, doi:10.1029/2005JB003862 (2006).

8. Brodsky, E. E. & Kanamori, H. Elastohydrodynamic lubrication of faults. *J. Geophys. Res.* **106**, No. B8, 16, 357–16, 374 (2001).
9. Bizzarri, A. The mechanics of lubricated faults: Insights from 3-D numerical models. *J. Geophys. Res.* **117**, B05304, doi:10.1029/2011JB008929 (2012).
10. Nur, A. & Booker, J. Aftershocks caused by pore fluid flow? *Science* **175**, 885–887 (1972).
11. Miller, S. A., Nur, A. & Olgaard, D. L. Earthquakes as a coupled shear stress-high pore pressure dynamical system. *Geophys. Res. Lett.* **23**, 197–200 (1996).
12. Miller, S. A. *et al*. Aftershocks driver by high-pressure CO_2 source at depth. *Nature* **427**, 724–727 (2004).
13. Yamashita, T. Simulation of seismicity due to fluid migration in a fault zone. *Geophys. J. Int.* **132**, 661–675 (1998).
14. Shapiro, S. A., Patzig, R., Rothert, E. & Rindshwentner, J. Triggering of seismicity by pore-pressure perturbations: Permeability-related signature of the phenomenon. *Pure Appl. Geophys.* **160**, 1051–1066 (2003).
15. Davies, R., Foulgera, G., Bindleya, A. & Styles, P. Induced seismicity and hydraulic fracturing for the recovery of hydrocarbons. *Marine and Petroleum Geology* **45**, 171–185 (2013).
16. Hitzman, M. W. *et al. Induced Seismicity Potential in Energy Technologies.* The National Academies Press, Washington DC, 248 pp. (2013).
17. Liu, S., Xu, L. & Talwani, P. Reservoir induced seismicity in the Dajangkou Reservoir: a quantitative analysis. *Geophys. J. Int.* **185**, 514–526 (2011).
18. Simpson, D. W., Leith, W. S. & Scholz, C. H. Two types of reservoir–induced seismicity. *Bull. Seism. Soc. Am.* **78**, No. 6, 2025–2040 (1988).
19. Redmayne, D. W. Mining induced seismicity in UK coalfields identified on the BGS National Seismograph Network. *Geological Society, London, Engineering Geology Special Publications* **5**, 405–413.
20. Gupta, H. K. A review of recent studies of triggered earthquakes by artificial water reservoirs with special emphasis on earthquakes in Koyna, India. *Earth-Science Reviews* **58**, 279–310 (2002).
21. Mekkawi, M., Grasso, J. R. & Schnegg, P. A. A long-lasting relaxation of seismicity at Aswan reservoir, Egypt, 1982-2001. *Bull. Seism. Soc. Am.* **94**, 479–492 (2004).
22. Eagar, K. C., Pavlis, G. L. & Hamburger, M. W. Evidence of possible induced seismicity in the Wabas Valley seismic zone from improved microearthquake locations *Bull. Seism. Soc. Am.* **96**, 1718–1728 (2006).
23. Gomberg, J., Beeler, N. & Blanpied, M. On rate-state and Coulomb failure models. *J. Geophys. Res.* **105**, 7557–7871 (2000).
24. Belardinelli, M. E., Bizzarri, A. & Cocco, M. Earthquake triggering by static and dynamic stress changes. *J. Geophys. Res.* **108**, No. B3, 2135, doi:10.1029/2002JB001779 (2003).
25. Dahm, T. How to discriminate induced, triggered and natural seismicity, *Proceedings of the Workshop Induced seismicity*, *Centre Européen de Géodynamique et de Séismologie*, 69–76 (2010).
26. Davis, S. D. & Frohlich, C. Did (or will) fluid injection cause earthquakes? Criteria for a rational assessment. *Seism. Res. Lett.* **64**, 207–224 (1993).
27. Gupta, H. K., Rastogi, B. K. & Narain, H. Common features of reservoir associated seismic acrivities. *Bull. Seismol. Soc. Am.* **62**, 481–492 (1972).
28. Kerr, R. A. & Stone, R. A Human trigger for the great quake of Sichuan? *Science* **323**, 322 (2009).
29. Ge, S. *et al*. Did the Zipingpu Reservoir trigger the 2008 Wenchuan earthquake? *Geophys. Res. Lett.* **36**, L20315, doi:10.1029/2009GL040349 (2009).
30. Deng, Z. *et al*. Evidence that the 2008 M_w 7.9 Wenchuan earthquake could not have been induced by the Zipingpu Reservoir. *Bull. Seism. Soc. Am.* **100**, 2805–2814, doi:10.1785/0120090222 (2010).
31. Hsieh, P. A. & Bredehoeft, J. D. A reservoir analysis of the Denver earthquakes: A case of induced seismicity. *J. Geophys. Res.* **86**, No. 2, 903–920 (1981).
32. Caloi, P. *et al*. Terremoti della Val Padana del 15-16 maggio 1951. *Ann. Geofis.* **9**, 63–95 (1956).
33. ICHESE, International Commission on Hydrocarbon Exploration and Seismicity in the Emilia Region, Report on the hydrocarbon exploration and seismicity the Emilia region. http://geo.regione.emilia-romagna.it/gstatico/documenti/ICHESE/ICHESE_Report.pdf (2014).
34. Cartlidge, E. Human activity may have triggered fatal Italian earthquakes, Panel says. *Science* **344**, 141 (2014).
35. Byerlee, J. Friction of rocks. *Pure Appl. Geophys.* **116**, 615–626 (1978).
36. Zoback, M. D. *et al*. New evidence of the state of stress of the San Andreas fault system. *Science* **238**, 1105–1111, doi:10.1126/science.238.4830.1105 (1987).
37. Raesenberg, P. A. & Simpson, R. W. Response of regional seismicity to the static stress change produced in the Loma Prieta earthquake. *Science* **255**, 1687–1690 (1992).
38. Iio, Y. Frictional coefficient on faults in a seismogenic region inferred from earthquake mechanism solutions. *J. Geophys. Res.* **102**, No. B3, 5403–5412 (1997).
39. Yamamoto, K. & Yabe, Y. Stresses at sites close to the Nojima Fault measured from core samples. *The Island Arc* **10**, 266–281 (2001).
40. Yamamoto, K., Sato, N. & Yabe, Y. Elastic property of damaged zone inferred from in-situ stresses and its role on the shear strength of faults. *Earth Planets Space* **54**, 1181–1194 (2002).
41. Kubo, A. & Fukuyama, E. Stress fields and fault reactivation angles of the 2000 western Tottori aftershocks and the 2001 northern Hyogo swarm in southwest Japan. *Tectonophys.* **378**, 223–239 (2004).
42. Rydelek, P. A. & Sacks, I. S. Large earthquake occurrence affected by small stress changes. *Bull. Seismol. Soc. Am.* **89**, 822–828 (1999).
43. Felzer, K. R. & Brodsky, E. E. Decay of aftershock density with distance indicates triggering by dynamic stress. *Nature* **441**, 735–738 (2006).
44. Terzaghi, K., Peck, R. B. & Mesri, G. *Soil Mechanics in Engineering Practice,* 3rd Ed., John Wiley, Hoboken, N. J. (1996).
45. Mulargia, F. & Geller, R. J. *Earthquake science and seismic risk reduction.* Kluwer, Dordrecht, The Netherlands, 338 pp. (2003).
46. Talwani, P., Chen, L. & Gahalaut, K. Seismogenic permeability, k_s. *J. Geophys. Res.* **112**, B07309, doi:10.1029/2006JB004665 (2007).
47. Dieterich, J. H. Time-dependent friction as a possible mechanism for aftershocks. *J. Geophys. Res.* **77**, No. 20, 3771–3781 (1972).
48. Marone, C. The effect of loading rate on static friction and the rate of fault healing during the earthquake cycle. *Nature* **391**, 69–72 (1998).
49. Nakatani, M. A new mechanism of slip weakening and strength recovery of friction associated with the mechanical consolidation of gouge. *J. Geophys. Res.* **103**, No. B11, 27, 239–27, 256 (1998).
50. Raleigh, C. B., Healy, J. H. & Bredehoeft, J. D. Faulting and crustal stress at Rangely, Colorado. *Am. Geophys.l Un. – Geophysical Monograph Series* **16**, 275–284 (1972).
51. Raleigh, C. B., Healy, J. H. & Bredehoeft, J. D. An experiment in earthquake control at Rangely, Colorado. *Science* **191**, 1230–1237 (1976).
52. Talebi, S. & Boone, T. J. Source parameters of injection-induced microseismicity. *Pure Appl. Geophys.* **153**, 113–130 (1998).
53. Stein, R. S. Tidal triggering caught in act. *Nature* **402**, 605–609, doi:10.1038/45144 (1999).
54. Zoback, M. D. & Healy, J. H. In situ stress measurements to 3.5 km depth in the Cajon Pass scientific research borehole: Implications for the mechanics of crustal faulting. *J. Geophys. Res.* **97**, No. B4, 5039–5057 (1992).
55. Yang, S., Huang, L., Xie, F., Cui, X.& Yao, R. Quantitative analysis of the shallow crustal tectonic stress field in China mainland based on in situ stress data. *J. Asian Earth Sci.* **85**, 154–162 (2014).
56. The World Stress Map Project, http://dc-app3-14.gfz-potsdam.de/pub/introduction/introduction_frame.html.
57. Bizzarri, A. On the deterministic description of earthquakes. *Rev. Geophys.* **49**, RG3002, doi:10.1029/2011RG000356 (2011).
58. Kanamori, H. The energy release in great earthquakes. *J. Geophys. Res.* **82**, No. 20, 2981–2987, doi:10.1029/JB082i020p02981 (1977).
59. Anooshelpoor, A. & Brune, J. N. Quasi-static slip-rate shielding by locked and creeping zones as an explanation for small repeating earthquakes at Parkfield. *Bull. Seism. Soc. Am.* **91**, 401–403 (2001).
60. Hainzl, S., Kraft, T., Wassermann, J., Igel, H. & Schmedes, E. Evidence for rainfall triggered earthquake activity. *Geophys. Res. Lett.* **33**, L19303, doi:10.1029/2006GL027642 (2006).
61. Biot, M. A. General solutions of the equationsof elasticity and consolidation for a porous material. *J. Appl. Mech.* **23**, 91–96 (1956).
62. Rice, J. R. & Cleary, M. P. Some basic stress diffusion solutions for fluid-saturated elastic porous media with compressible constituent. *Rev. Geohpys. and Space Phys.* **14**, No. 2, 227–241 (1976).
63. Roeloffs, E. A. Fault stability changes induced beneath a reservoir with cyclic variations in water level. *J. Geophys. Res.* **83**, 2107–2124 (1988).
64. Roeloffs, E. A. Poroelastic techniques in the study of earthquake- related hydrologic phenomena. *Adv. Geophys.* **37**, 136–195 (1996).
65. Durà-Gomez, I. & Talwani, P. Reservoir induced seismicity associated with the Itoiz Reservoir, Spain: a case study. *Geophys. J. Int.* **181**, 343–356 (2010).
66. Sieh, K. A review of geological evidence for recurrence times of large earthquakes: in *Earthquake Prediction — An International Review*, Maurice Ewing Series 4, pp. 181–207. Reprinted in Chinese in *Collected Translations in Seismology and Geology* 6, No. 6, pp. 32–38, Seismological Press, State Seismological Bureau, Beijing (1981).
67. Sieh, K., Stuiver, M. & Brillinger, D. A more precise chronology of earthquakes produced by the San Andreas fault in southern California. *J. Geophys. Res.* **94**, 603–623 (1989).
68. Mulargia, F. Why next earthquake will be a big surprise. *Bull. Seism. Soc. Am.* **103**, No. 5, 2946–2952 (2013).
69. Kanamori, H. & Anderson, D. L. Theoretical bases of some empirical relations in seismology. *Bull. Seism. Soc. Am.* **65**, 1073–1095 (1975).
70. Cotton, F., Archuleta, R.& Causse, M. What is sigma of the stress drop? *Seismol. Res. Lett.* **84**, 42–48 (2012).
71. Pakiser, L. C., Eaton, J. P., Healy J. H, & Raleigh, C. B. Earthquake prediction and control. *Science* **166**, 1467–1474 (1969).
72. Healy, J. H., Rubey, W. W., Griggs, D. T. & Raleigh, C. B. The Denver earthquakes.*Science* **161**, No. 3848, 1301–1310 (1968).
73. Ohtake, M. Seismic activity induced by water injection at Matsushiro, Japan. *J. Phys. Earth* **22**, 163–176 (1974).
74. Rutledge, J. T., Phillips, W. S. & Mayerhofer, M. J. Faulting induced by forced fluid injection and fluid flow forced by faulting: An interpretation of hydraulic-fracture microseismicity, Carthage Cotton valley gas giield, Texas. *Bull. Seism. Soc. Am.* **94**, No. 5, 1817–1830 (2004).
75. Frohlich, C. Two-year survey comparing earthquake activity and injection-well locations in the Barnett Shale, Texas. *Proc. Nat. Acad. Sci.* **109**, No. 35, 13,934–13,938, doi:10.1073/pnas.1207728109 (2012).
76. Ellsworth, W. L. Injection-induced earthquakes. *Science* **314**, 1225942, doi:10.1126/science. 1225942 (2013).

77. van der Elst, N. J., Savage, H. M., Keranen, K. M. & Abers, G. A. Enhanced remote earthquake triggering at fluid-injection sites in the Midwestern United States. *Science* **141**, No. 6142, 164–167, doi:10.1126/science.1238948 (2013).

Author contributions

F.M. and A.B. developed the Physics. F.M. performed the numerical simulations. F.M. and A.B. wrote the paper.

Additional information

Competing financial interests: The authors declare no competing financial interests.

How to cite this article: Mulargia, F. & Bizzarri, A. Anthropogenic Triggering of Large Earthquakes. *Sci. Rep.* **4**, 6100; DOI:10.1038/srep06100 (2014).